A Simplified Hemispherical 2-D Angular Space Null Steering Approach for Linearly Polarization

Yue Li, *Member, IEEE*, Zhijun Zhang, *Senior Member, IEEE*, Changjiang Deng, *Student Member, IEEE*, and Zhenghe Feng, *Fellow, IEEE*

Abstract—A simplified two-dimensional (2-D) angular space null steering approach is presented in this letter for the linearly polarized (LP) null reconfigurable antenna (NRA) applications. In the proposed approach, a deep null of linear polarization in the radiation pattern can be achieved by combining a corner truncated patch with an omnidirectional radiating monopole. By tuning the amplitude ratio and phase difference of the two input signals, the resulting radiation pattern is able to generate a gain null that is steerable in the elevation and azimuth planes. Compared to the previous reported antenna structures, the proposed approach is easy in fabrication without using switching components. For the first time, we experimentally demonstrate the proposed approach by analyzing the null depth and the steering angle range.

Index Terms—2-D anti-interference, null steering, pattern-reconfigurable antennas.

I. INTRODUCTION

IN THE modern cognitive radio systems, null reconfigurable antennas (NRAs) are widely adopted for their merits of suppressing interference signals. Null depth and steering angle range are the two most important factors. Null steering technique is first studied in the array applications by changing the feeding weight of an individual antenna element with different optimization algorithms [1]–[4]. In the recent literature, null steering method is also developed using a single antenna without large physical dimensions [5]–[9]. For example, a number of varactors are integrated with parasitic patches for one-dimensional (1-D) [7] and two-dimensional (2-D) [8] angular space linear polarized (LP) null steering applications. The usage of the varactors and their bias circuit will make the overall system complex and introduce more loss. In the work of [9], the patch array is utilized to achieve circularly polarized (CP) null steering capability.

In this letter, we mainly focus on the LP null steering application and propose a null steering approach for 2-D angular space scan application in the upper hemisphere. In this approach, a broadside radiation pattern and an azimuthally omnidirectional radiation pattern are employed for continuous null scanning capability. The monopole provides an LP field in 2-D angular space. A field with identical polarization is needed in the same 2-D angular space for cancellation (achieving null). Therefore, we used a CP patch antenna to provide rotated field for this purpose. By combining these two radiation patterns with tunable input amplitude ratio and phase difference, null steering capability is achieved in both the elevation and the azimuth planes for the LP components. Compared to the previous work [7], [8], the proposed NRA has the merits of simple structure, wide steering angle, easy fabrication, and low cost. We also experimentally demonstrated the proposed LP null steering approach by using measured field values for the first time. The measured results show the excellent 2-D angular space LP null steering capability.

II. ANTENNA DESIGN AND SIMULATION

A patch-monopole integrated antenna has been built to achieve the design approach, as shown in Fig. 1. The detailed values of each parameter are listed in Table I. The antenna is composed of a corner-truncated patch with the broadside pattern and a monopole with the omnidirectional pattern. A Teflon substrate is used to support the patch, with a relative permittivity of 2.65 and a tangent loss of 0.002. The thickness of the substrate is 2 mm. The monopole is positioned at the center of the patch, with a length of 28.5 mm and diameter of 3 mm. The patch antenna is fed through port 1, and the monopole is fed through port 2. The patch-monopole feeding structure is based on [10] and [11], but the patch is for circular polarization. The hybrid antenna is operating at the frequency of 2.4 GHz. At 2.4 GHz, the magnitudes of reflection coefficients of ports 1 and 2 are -18.3 and -12.5 dB, and the isolation between ports 1 and 2 is 22.27 dB. The simulated axial ratio of the patch is 0.82 dB at this operating frequency.

Antennas selection for field cancellation is important to this idea. We aim to achieve null for linear polarization in 2-D angular space. The monopole radiates azimuthally symmetrical LP field (E_θ) in 2-D angular space. If we use an ordinary patch (without corner cutting), we only achieve null in the xz-plane. For example, in $+y$-direction, the field radiated from the patch is orthogonal with the field radiated from the monopole. What we need is an antenna providing the identical field (E_θ) with the monopole in 2-D angular space. Therefore, a rotating field antenna is used for the field cancellation. The corner truncated
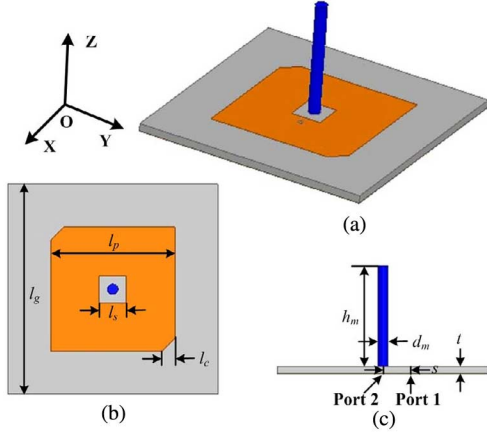
Fig. 1. Geometry of the proposed 2-D angular space null steering antenna: (a) 3-D view; (b) top view; (c) side view.
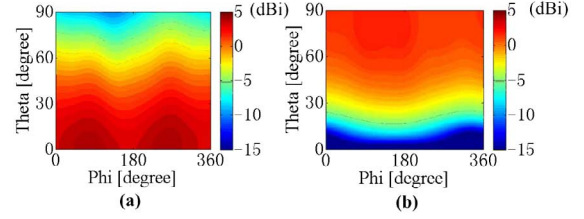

Fig. 2. Simulated gain distributions at 2.4 GHz: (a) CP patch; (b) monopole.
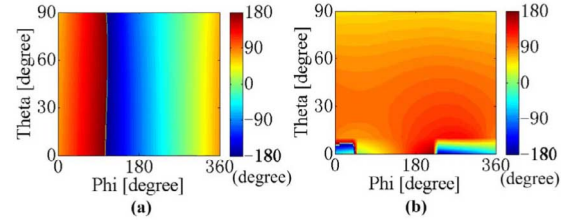
Fig. 3. Simulated phase distributions at 2.4 GHz: (a) CP patch; (b) monopole.

TABLE I
DETAILED DIMENSIONS (UNIT: MILLIMETERS)

l_g	l_p	l_c	l_s	h_m	s	d_m	t
60	35.5	3.8	7.8	28.5	6.4	3	2

patch with CP field is the easiest way for the practical system. In this arrangement, the null is achieved only for linear polarization of E_θ.

Here, we will theoretically analyze the simplified 2-D angular space null steering approach for E_θ using two feeding ports. Without loss of generality, for the broadside radiated antenna (patch), the normalized radiating field distribution is $E_b(\theta, \varphi)$, with the input amplitude A_1 and phase Ψ_1. For the omnidirectional radiated antenna (monopole), the normalized radiating field distribution is $E_o(\theta, \varphi)$, with the input amplitude A_2 and phase Ψ_2. For the time convention field, the combined field at (θ, φ) can be written as

$$E_{\text{total}}(\theta, \varphi) = A_1 E_b(\theta, \varphi)e^{(j\omega t + \Psi_1)} + A_2 E_o(\theta, \varphi)e^{(j\omega t + \Psi_2)} \tag{1}$$

where $E_b(\theta, \varphi) = E_b(\theta)e^{j\varphi'(\varphi)}$ for the CP patch, with the φ-symmetrical broadside rotating field, and $E_o(\theta, \varphi) = E_o(\theta)$ for the monopole, with the omnidirectional radiating field. $\varphi'(\varphi)$ is the phase distribution according to φ. Therefore, (1) can be written as

$$E_{\text{total}}(\theta, \varphi) = A_1 E_b(\theta)e^{(j\omega t + \varphi'(\varphi) + \Psi_1)} + A_2 E_o(\theta)e^{(j\omega t + \Psi_2)}. \tag{2}$$

To achieve a null at (θ_0, φ_0) for the combined field, $E_{\text{total}}(\theta_0, \varphi_0)$ should be equal to zero. Therefore, the following two equations must be satisfied:

$$A_1 E_b(\theta_0) = A_2 E_o(\theta_0) \tag{3}$$
$$\Psi_2 - \Psi_1 = \varphi'(\varphi) + (2n + 1)\pi. \tag{4}$$

For a desired null angle of (θ_0, φ_0), the $E_b(\theta_0)$ and $E_o(\theta_0)$ in (3) are known, and $\varphi'(\varphi)$ in (4) is also known. By tuning the ratio of A_1 and A_2, (3) can be satisfied. By tuning the difference of Ψ_1 and Ψ_2, (4) can be satisfied. Therefore, the null can be achieved at theoretical arbitrary (θ, φ), which is determined by the field distribution of the combined field $E_b(\theta, \varphi)$ and $E_o(\theta, \varphi)$.

TABLE II
SIMULATED NULL DEEP (UNIT: DB) AND STEERING ANGLE (θ_0, φ_0)

Phase \ Amp.	$\Psi_2 - \Psi_1 = 0°$	$\Psi_2 - \Psi_1 = 90°$	$\Psi_2 - \Psi_1 = 180°$	$\Psi_2 - \Psi_1 = 270°$
$A_2/A_1 = 1/4$	-29.9 dB (90°, 152°)	-25.8 dB (90°, 248°)	-23.2 dB (90°, 344°)	-28.2 dB (90°, 76°)
$A_2/A_1 = 1/2$	-47.7 dB (70°, 173°)	-47.6 dB (82°, 254°)	-50.6 dB (76°, 356°)	-56.1 dB (72°, 90°)
$A_2/A_1 = 1/1$	-51.9 dB (45°, 195°)	-48.1 dB (53°, 285°)	-45.9 dB (50°, 12°)	-43.9 dB (46°, 109°)
$A_2/A_1 = 2/1$	-49.3 dB (24°, 207°)	-47.4 dB (31°, 299°)	-50.1 dB (30°, 16°)	-56.8 dB (25°, 112°)
$A_2/A_1 = 4/1$	-54.8 dB (12°, 219°)	-44.7 dB (18°, 306°)	-44.2 dB (16°, 13°)	-43.8 dB (12°, 105°)

As discussed above, in order to achieve the null at a desired angle (θ_0, φ_0), we need to know the amplitude and phase of the electric fields of the CP patch and the monopole at (θ_0, φ_0), which are shown in Figs. 2 and 3. The simulated angle range is 0° to 90° for θ, and 0° to 360° for φ. For the CP patch, the radiation pattern is φ-symmetrical and unidirectional. The phase distribution is shown in Fig. 3(a). The phase center is selected in the center of the patch. Along the θ-direction, the phase is nearly uniform. Along the φ-direction, the phase increases with φ. For the monopole, the phase distribution is nearly uniform in the full space, as shown in Fig. 3(b).

Then, we tune the amplitude ratio and phase difference of the two input signals, which are fed at the two ports. The amplitudes of the electric fields radiated by the two antennas are controlled by tuning A_2/A_1. Out of phase of two electric fields is achieved by tuning the phase difference $\Psi_2 - \Psi_1$. Therefore, a null of gain appears at the desired angle (θ_0, φ_0). We have simulated the null steering angle and the normalized null depth with different input phase differences ($\Psi_2 - \Psi_1 = 0°$, 90°, 180°, and 270°), and different input amplitude ratios ($A_2/A_1 = 1/4$, 1/2, 1/1, 2/1, and 4/1). The simulated results are listed in Table II. Among these results, three different electric field distributions are depicted in Figs. 4–6 as examples. The first one is with $A_2/A_1 = 1/2$, $\Psi_2 - \Psi_1 = 90°$; the second one is with $A_2/A_1 = 1/1$,
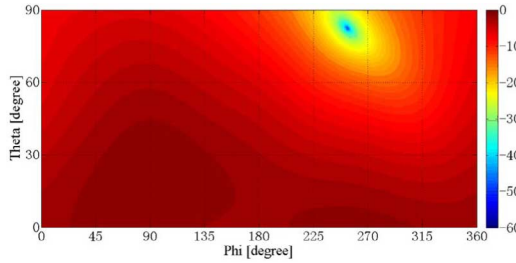
Fig. 4. Simulated normalized electric field (E_θ) magnitude distribution with null at 2.4 GHz when $A_2/A_1 = 1/2$ and $\Psi_2 - \Psi_1 = 90°$. The scale is in decibels.
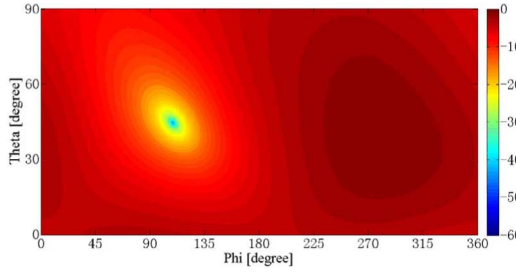

Fig. 5. Simulated normalized electric field (E_θ) magnitude distribution with null at 2.4 GHz when $A_2/A_1 = 1/1$ and $\Psi_2 - \Psi_1 = 270°$. The scale is in decibels.
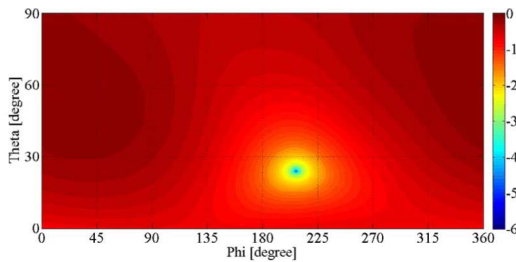

Fig. 6. Simulated normalized electric field (E_θ) magnitude distribution with null at 2.4 GHz when $A_2/A_1 = 2/1$ and $\Psi_2 - \Psi_1 = 0°$. The scale is in decibels.

$\Psi_2 - \Psi_1 = 270°$; and the third one is with $A_2/A_1 = 2/1$, $\Psi_2 - \Psi_1 = 0°$. In Fig. 4, the null appears at the direction of $(82°, 254°)$ with a normalized depth of 47.6 dB. In Fig. 5, the null appears at the direction of $(46°, 109°)$ with a normalized depth of 43.9 dB. In Fig. 6, the null appears at the direction of $(24°, 207°)$ with a normalized depth of 49.3 dB.

III. EXPERIMENT VERIFICATION

The antenna prototype has been built and tested for an anti-interference system. We focus on the performance at the two feeding ports. In the measurement, we measured the magnitude and phase of the E_θ of the two antennas and combined them using the software of MATLAB by changing the input magnitude and phase difference of two feeding ports.

The operating frequency shifts higher than simulation due to the smaller value of substrate permittivity. We have found that the best axial ratio is at 2.43 GHz with the value of 1.24 dB. Therefore, we choose 2.43 GHz to check the performance. At 2.43 GHz, the return losses of ports 1 and 2 are 16.6 and 14.3 dB, and the port isolation is 25.8 dB.

The gain distributions in the upper hemisphere of both antennas at 2.43 GHz are shown in Fig. 7. Clearly, a broadside
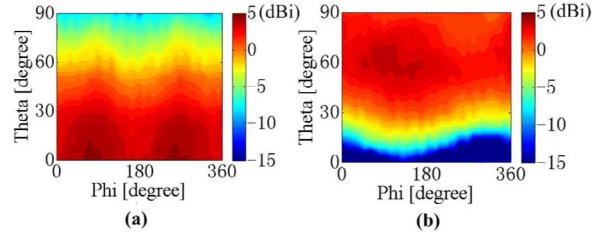

Fig. 7. Measured gain distributions at 2.43 GHz: (a) CP patch; (b) monopole.
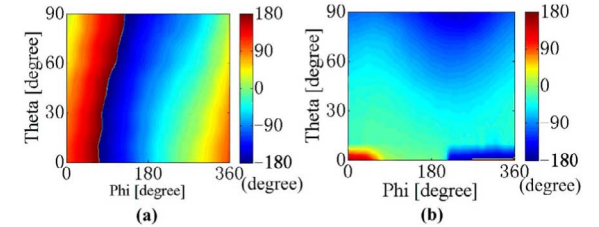

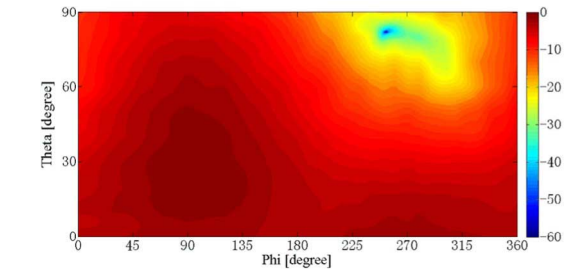Fig. 8. Measured phase distributions at 2.43 GHz: (a) CP patch; (b) monopole.

Fig. 9. Measured normalized electric field (E_θ) magnitude distribution with null at 2.43 GHz when $A_2/A_1 = 1/2$ and $\Psi_2 - \Psi_1 = 90°$. The scale is in decibels.

pattern and an omnidirectional pattern are achieved and with the measured gain of 4.74 and 3.45 dBi, respectively. We can obtain the normalized magnitude distributions of the radiated electric fields from Fig. 7. The phase distributions of both antennas are illustrated in Fig. 8. The two antennas are measured in the same position with the same phase center as simulation. For the CP patch in Fig. 8(a), the interphase with equal phase values is tilted, compared to the simulation in Fig. 3(a). This is due to the phase center changes at different θ in the measurement. This will conclude that both θ and φ change with different input phase difference $\Psi_2 - \Psi_1$. As shown in Fig. 8(b), the phase is almost uniform for the monopole, which agrees well with the results in Fig. 3(b). In the measurement, the two antennas are fed using different cables with different lengths. In the pattern combination, we evaluated and compensated this extra phase difference.

Based on the measured radiation pattern data, we calculated the null steer angle and null depth. The measured results are listed in Table III. We use different input phase differences ($\Psi_2 - \Psi_1 = 0°, 90°, 180°,$ and $270°$) and different input amplitude ratios ($A_2/A_1 = 1/4, 1/2, 1/1, 2/1,$ and $4/1$). As comparisons to Figs. 4–6, we have shown the measured results in Figs. 9–11. In Fig. 9, the input magnitude ratio is 1/2, and the phase difference is $90°$. The null appears at the direction of $(83°, 254°)$ with a normalized depth of 56.3 dB. In Fig. 10, the input magnitude ratio is 1/1, and the phase difference is $270°$. The null appears at the direction of $(83°, 254°)$ with a

Fig. 10. Measured normalized electric field (E_θ) magnitude distribution with null at 2.43 GHz when $A_2/A_1 = 1/1$ and $\Psi_2 - \Psi_1 = 270°$. The scale is in decibels.
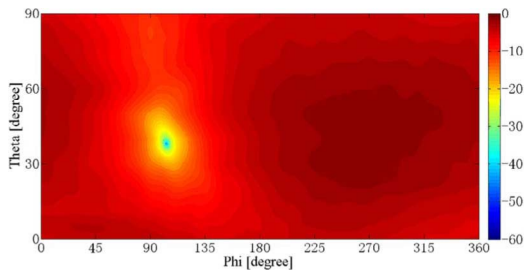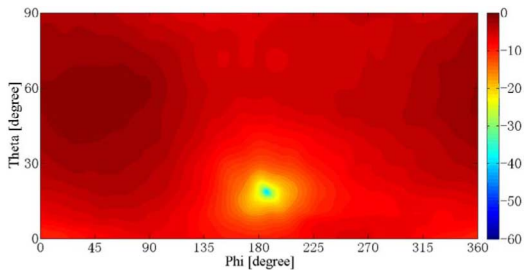

Fig. 11. Measured normalized electric field (E_θ) magnitude distribution with null at 2.43 GHz when $A_2/A_1 = 2/1$ and $\Psi_2 - \Psi_1 = 0°$. The scale is in decibels.
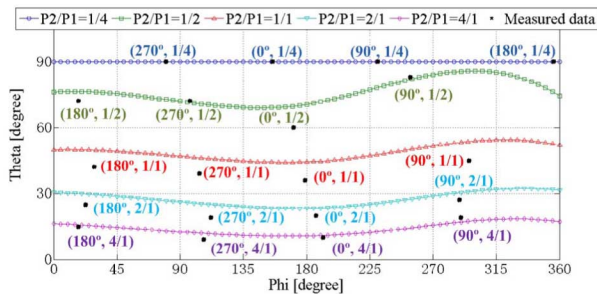

Fig. 12. Measured null steering angles with different ($\Psi_2 - \Psi_1$, A_2/A_1) and the simulated curves.

TABLE III
MEASURED NULL DEEP (UNIT: DECIBELS) AND STEERING ANGLE (θ_0, φ_0)

Phase / Amp.	$\Psi_2 - \Psi_1 = 0°$	$\Psi_2 - \Psi_1 = 90°$	$\Psi_2 - \Psi_1 = 180°$	$\Psi_2 - \Psi_1 = 270°$
$A_2/A_1 = 1/4$	-26.8 dB (90°, 156°)	-25.0 dB (90°, 231°)	-26.0 dB (90°, 356°)	-22.4 dB (90°, 80°)
$A_2/A_1 = 1/2$	-45.2 dB (60°, 171°)	-56.3 dB (83°, 254°)	-61.5 dB (72°, 18°)	-54.6 dB (72°, 97°)
$A_2/A_1 = 1/1$	-46.8 dB (36°, 179°)	-53.2 dB (45°, 296°)	-44.5 dB (42°, 29°)	-47.4 dB (39°, 104°)
$A_2/A_1 = 2/1$	-40.5 dB (20°, 187°)	-48.4 dB (27°, 289°)	-43.9 dB (25°, 23°)	-41.1 dB (19°, 112°)
$A_2/A_1 = 4/1$	-39.3 dB (10°, 192°)	-43.0 dB (19°, 290°)	-41.6 dB (15°, 18°)	-41.3 dB (9°, 107°)

normalized depth of 47.4 dB. In Fig. 11, the input magnitude ratio is 2/1, and the phase difference is 0°. The null appears at the direction of (27°, 189°) with a normalized depth of 48.4 dB.

To illustrate the 2-D angular space null steering angle range, we plot the results listed in Table III. As shown in Fig. 12, five

curves with different input amplitude ratios are simulated results, and the black points are based on the measured results with different ($\Psi_2 - \Psi_1$, A_2/A_1). The measured null angles have a smaller value of θ, especially for the elevation angle range of 20°–60°. This can be explained from the gain distribution of the monopole in Fig. 7(b). The beam is tilted toward the $+z$-axis as caused by the unwanted diffraction from the edges of the ground. The measured null angles fluctuate in a larger range than the simulated curves. This can be explained in Figs. 7(a) and 8(a). At 2.43 GHz, the measured axial ratio is larger than the simulation. The null scanning angle is not strictly uniformly distributed by input phase difference $\Psi_2 - \Psi_1$. This is due to the asymmetrical structure of the corner-truncated patch.

As shown in Fig. 12, we talk about the sensitivity of achieved null angle with the input magnitude ratio and the phase difference. In the azimuthal plane, the angle φ_0 is dictated by the phase difference of $\Psi_2 - \Psi_1$. In the elevated plane, the sensitivity of angle θ_0 to the magnitude ratio A_2/A_1 is different. The achieved direction of null for smaller value of θ_0 is less sensitive than that of larger value of θ_0, due to the field distribution of the two antennas.

IV. CONCLUSION

In this letter, we have presented a simplified 2-D angular space linearly polarized null steering approach based on the pattern combination. In the proposed approach, a CP broadside pattern and an omnidirectional pattern are combined with a tunable input amplitude ratio and phase difference. We have experimentally demonstrated the proposed approach for the first time using measured field values. The measured results have shown good null steering capability with deep null. The achievable speed of null steering is determined by the amplifier (tuning amplitude) and the phase shifter (tuning phase).

REFERENCES

[1] C. Ko, "A fast null steering algorithm for linearly constrained adaptive arrays," *IEEE Trans. Antennas Propag.*, vol. 39, no. 8, pp. 1098–1104, Aug. 1991.
[2] M. Dawoud and T. Ismail, "Experimental verification of null steering by element position perturbations," *IEEE Trans. Antennas Propag.*, vol. 40, no. 11, pp. 1431–1434, Nov. 1992.
[3] T. Vu, "On null steering in rectangular planar array," *IEEE Trans. Antennas Propag.*, vol. 40, no. 8, pp. 995–997, Aug. 1992.
[4] M. Sharawi and D. Aloi, "Null steering approach with minimized PCV and GD for large aperture vertical antenna arrays," *IEEE Trans. Antennas Propag.*, vol. 55, no. 7, pp. 2120–2123, Jul. 2007.
[5] M. Parihar, A. Basu, and S. Koul, "Efficient spurious rejection and null steering using slot antennas," *IEEE Antennas Wireless Propag. Lett.*, vol. 10, pp. 207–210, 2011.
[6] M. Parihar, A. Basu, and S. Koul, "Slot antenna with reconfigurable null scanning," in *Proc. AEMC*, 2009, pp. 1–4.
[7] S. Yong and J. Bernhard, "A pattern reconfigurable null scanning antenna," *IEEE Trans. Antennas Propag.*, vol. 60, no. 10, pp. 4538–4544, Oct. 2012.
[8] S. Yong and J. Bernhard, "Reconfigurable null scanning antenna with three dimensional null steer," *IEEE Trans. Antennas Propag.*, vol. 61, no. 3, pp. 1063–1070, Mar. 2013.
[9] W. Cheuk, M. Trinkle, and D. Gary, "Null-Steering LMS dual-polarised adaptive antenna arrays for GPS," *J. Global Positioning Syst.*, vol. 4, no. 1–2, pp. 258–267, 2005.
[10] N. Kuga and H. Arai, "Feeding condition of patch-monopole composite antenna with horizontal broad beam," in *Proc. APMC*, Taiwan, 2001, pp. 1358–1361.
[11] G. Sanford and H. Hwang, "Antenna structures including orthogonally oriented antennas and related communications devices," US Patent 6313801, Nov. 6, 2001.